J Therm Anal Calorim (2013) 111:9–16
DOI 10.1007/s10973-011-2104-6

Magnetic properties of nanocrystalline $CuFe_2O_4$ and kinetics of thermal decomposition of precursor

Xuehang Wu · Kaiwen Zhou · Wenwei Wu · Xuemin Cui · Yongni Li

Received: 27 October 2011 / Accepted: 22 November 2011 / Published online: 10 December 2011

Abstract $CuFe_2(C_2O_4)_3{\cdot}4.5H_2O$ was synthesized by solid-state reaction at low heat using $CuSO_4{\cdot}5H_2O$, $FeSO_4{\cdot}7H_2O$, and $Na_2C_2O_4$ as raw materials. The spinel $CuFe_2O_4$ was obtained via calcining $CuFe_2(C_2O_4)_3{\cdot}4.5H_2O$ above 400 °C in air. The $CuFe_2(C_2O_4)_3{\cdot}4.5H_2O$ and its calcined products were characterized by thermogravimetry and differential scanning calorimetry, Fourier transform FT-IR, X-ray powder diffraction, scanning electron microscopy, energy dispersive X-ray spectrometer, and vibrating sample magnetometer. The result showed that $CuFe_2O_4$ obtained at 400 °C had a saturation magnetization of 33.5 emu g^{-1}. The thermal process of $CuFe_2(C_2O_4)_3{\cdot}4.5H_2O$ experienced three steps, which involved the dehydration of four and a half crystal water molecules at first, then decomposition of $CuFe_2(C_2O_4)_3$ into $CuFe_2O_4$ in air, and at last crystallization of $CuFe_2O_4$. Based on KAS equation, OFW equation, and their iterative equations, the values of the activation energy for the thermal process of $CuFe_2(C_2O_4)_3{\cdot}4.5H_2O$ were determined to be 85 ± 23 and 107 ± 7 kJ mol^{-1} for the first and second thermal process steps, respectively. Dehydration of $CuFe_2(C_2O_4)_3{\cdot}4.5H_2O$ is multistep reaction mechanisms. Decomposition of $CuFe_2(C_2O_4)_3$ into $CuFe_2O_4$ could be simple reaction mechanism, probable mechanism function integral form of thermal decomposition of $CuFe_2(C_2O_4)_3$ is determined to be $1 - (1 - \alpha)^{1/4}$.

X. Wu · K. Zhou · W. Wu (✉) · X. Cui · Y. Li
School of Chemistry and Chemical Engineering, Guangxi University, Nanning 530004, China
e-mail: gxuwuwenwei@yahoo.com.cn

K. Zhou
School of Materials Science and Engineering, Guangxi University, Nanning 530004, China

Keywords Nanoparticles · Ferrites · Chemical synthesis · Non-isothermal kinetics · Thermal process

Introduction

Spinels of the type $M^{2+}M_2^{3+}O_4$ attract the research interest because of their versatile practical applications [1–3]. In the case of M^{3+}=Fe, the resulting spinel ferrites having a general chemical composition of MFe_2O_4 (M = Cu, Mn, Mg, Zn, Ni, Co, etc.) are widely used in the field of high-density information storage, ferrofluids, catalysts, drug targeting, magnetic separation, magnetic resonance imaging, and gas sensor [4–11]. Within this group, copper ferrite ($CuFe_2O_4$) is very important soft magnetic material. Its properties such as magnetic behavior and gas-sensing properties are highly dependent on the synthesis method.

To date, various methods have been developed to synthesize $CuFe_2O_4$ with cubic structure, including ball-milling [12, 13], sol–gel synthesis [14], co-precipitation [15, 16], combustion synthesis [17], microwave synthesis [18], and solid-state reaction at low heat [4]. In the synthesis of $CuFe_2O_4$, it was found that crystallite diameter, morphology, and crystalline phases of $CuFe_2O_4$ associated with its properties were highly dependent on the synthesis method and temperature. Sun et al. [4] obtained spinel-type $CuFe_2O_4$ with a crystallite size of 75 nm by solid-state reaction at low heat when precursor was calcined at 600 °C. Tao et al. [16] studied synthesis of spinel-type $CuFe_2O_4$ via sol–gel and co-precipitation methods, respectively. The results showed that spinel-type $CuFe_2O_4$ was obtained at 600 °C via calcining precursor obtained by co-precipitation method. However, pure $CuFe_2O_4$ was not obtained until 800 °C by a sol–gel process, which might be due to the loose contact between copper and iron ions and

the possible low diffusion rate. Therefore, new synthesis methods for $CuFe_2O_4$ still need to be studied and innovated further. Besides, the mechanism and kinetics studies of thermal process of precursor are needed in order to obtain high-quality $CuFe_2O_4$ for practical applications.

The aim of this work is to prepare polycrystalline $CuFe_2O_4$ using $CuSO_4{\cdot}5H_2O$, $FeSO_4{\cdot}7H_2O$, and $Na_2C_2O_4$ as raw materials via solid-state reaction at low heat [11, 19] and to study magnetic properties of $CuFe_2O_4$, the mechanisms, and kinetics of the thermal process of precursor. The kinetics of the thermal process of precursor was studied using TG–DSC techniques. Non-isothermal kinetics of the thermal process of precursor was interpreted by the Kissinger–Akahira–Sunose (KAS) equation [20, 21] and Ozawa–Flynn–Wall (OFW) equation [22–24]. The kinetic (E_a mechanism) parameters of the thermal decomposition of $CuFe_2(C_2O_4)_3{\cdot}4.5H_2O$ are discussed for the first time.

Experimental

Reagent and apparatus

All chemicals were of reagent-grade purity. TG/DSC measurements were taken using a Netsch 40PC thermogravimetric analyzer. X-ray powder diffraction (XRD) was performed using a Rigaku D/max 2500 V diffractometer equipped with a graphite monochromator and a Cu target. The FT-IR spectra of the precursor and its calcined products were recorded on a Nexus 470 FT-IR instrument. The morphologies of the calcined samples and energy dispersive X-ray spectrometer (EDS) were obtained on S-3400 scanning electron microscopy (SEM). The specific saturation magnetizations (Ms) of the calcined sample powders were carried out at room temperature using a magnetic property measurement system (SQUID-MPMS-XL-5).

Preparation of $CuFe_2O_4$

The $CuFe_2O_4$ precursor was prepared by solid-state reaction at low heat using $CuSO_4{\cdot}5H_2O$, $FeSO_4{\cdot}7H_2O$, and $Na_2C_2O_4$ as raw materials at first. In a typical synthesis, $CuSO_4{\cdot}5H_2O$ (24.41 g), $FeSO_4{\cdot}7H_2O$ (54.37 g), $Na_2C_2O_4$ (43.24 g), and surfactant polyethylene glycol (PEG)-400 (3.0 mL, 50 vol%) were put in a mortar, and the mixture was fully ground by hand with a rubbing mallet for 40 min. The grinding velocity was about 200 circles/min, and the strength applied was moderate. The reactant mixture gradually became damp, and then, a paste formed quickly. The reaction mixture was kept at room temperature for 2 h. The mixture was washed with deionized water to remove soluble inorganic salts until SO_4^{2-} ion could not be visually detected with a 0.5 mol L^{-1} $BaCl_2$ solution. The solid was then washed with a small amount of anhydrous ethanol and dried at 86 °C for 4 h. The resulting material was subsequently determined to be the $CuFe(C_2O_4)_3{\cdot}4.5H_2O$. Nanocrystalline $CuFe_2O_4$ with cubic structure was obtained via calcining $CuFe(C_2O_4)_3{\cdot}4.5H_2O$ above 400 °C in air.

Determination of activation energy by KAS equation and OWF equation

Activation energy of thermal decomposition of solid compound can be obtained by KAS equation (Eq. 1) and OWF equation (Eq. 2), respectively.

$$\ln\frac{q}{T^2} = \ln\frac{AR}{g(\alpha)E_a} - \frac{E_a}{RT} \tag{1}$$

$$\ln q = \ln\frac{0.0048AE_a}{g(\alpha)R} - 1.0516\frac{E_a}{RT} \tag{2}$$

where q is the heating rate (K min^{-1}), T is the reaction temperature (K) in TG curve, E_a is the activation energy (kJ mol^{-1}) of thermal decomposition, R is the gas constant (8.314×10^{-3} kJ mol^{-1} K^{-1}), A is the pre-exponential factor, and α is called conversion degree. The $g(\alpha)$ is a function of α, and it reveals the mechanism of reaction. The plots of $\ln(q/T^2)$ versus $1/T$ and $\ln q$ versus $1/T$ corresponding to different conversions α can be obtained by a linear regression of least-square method, respectively. Thus, reaction activation energy E_a can be obtained from linear slope ($-E_a/R$, Eq. 1) and ($-1.0516E_a/R$, Eq. 2). In order to obtain exact E_a values of the thermal decomposition, the iterative equations of Eqs. 1 and 2 can be expressed as Eqs. 3 and 4, respectively [24].

$$\ln\frac{q}{h(x)T^2} = \ln\frac{AR}{g(\alpha)E_a} - \frac{E_a}{RT} \tag{3}$$

$$\ln\frac{q}{H(x)} = \ln\frac{0.0048AE_a}{g(\alpha)R} - 1.0516\frac{E_a}{RT} \tag{4}$$

where $h(x)$ is expressed by the fourth Senum and Yang approximation formulae [25]:

$$h(x) = \frac{x^4 + 18x^3 + 88x^2 + 96x}{x^4 + 20x^3 + 120x^2 + 240x + 120} \tag{5}$$

where $x = E_a/RT$, and $H(x)$ is equal to [24]:

$$H(x) = \frac{\exp(-x)h(x)/x^2}{0.0048\exp(-1.0516x)} \tag{6}$$

The iterative procedure performed involved the following steps: (i) assume $h(x) = 1$ or $H(x) = 1$ to estimate the initial value of the activation energy E_{a1}. The conventional isoconversional methods stop the calculation at this step; (ii) using E_{a1}, calculate a new

value of E_{a2} for the activation energy from the plot of $\ln[q/h(x)T^2]$ versus $1/T$ or $\ln[q/H(x)]$ versus $1/T$; (iii) repeat step (ii), replacing E_{a1} with E_{a2}. When $E_{ai} - E_{a(i-1)} < 0.1$ kJ mol^{-1}, the last value of E_i was considered to be the exact value of the activation energy of the reaction.

Determination of the most probably mechanism function

The probable mechanism function of thermal process, i.e., $g(\alpha)$ function, can be obtained by Eq. 7 [24]:

$$\ln g(\alpha) = \left[\ln\frac{AE_a}{R} + \ln\frac{e^{-x}}{x^2} + \ln h(x)\right] - \ln q \quad (7)$$

The procedure performed involved the following steps: (i) the conversion degrees α corresponding to multiple heating rates at the same temperature are put into the left of Eq. 7 at first, combined with twenty-six types of mechanism functions [26], and then the slope k and correlation coefficient r are obtained from the plot of $\ln[g(\alpha)]$ versus $\ln q$; (ii) $g(\alpha)$, which the value of the slope k is near to -1.00000 and correlation coefficient r is better, is determined to be the most probably mechanism function of thermal process.

Determination of pre-exponential factor A

The pre-exponential factor A can be estimated from the intercept of the plots of Eq. 2, inserting the most probable $g(\alpha)$ function determined [27].

Results and discussion

TG/DSC analysis of the precursor

Figure 1 shows the TG/DSC curves of $CuFe_2(C_2O_4)_3{\cdot}4.5H_2O$ at four different heating rates in air, respectively.

The TG/DSC curves show that thermal process of the $CuFe_2(C_2O_4)_3{\cdot}4.5H_2O$ below 450 °C occurs in three well-defined steps. For heating rate of 10 °C min^{-1}, the first step starts at about 50 °C, ends at about 201 °C, and characterized by a strong endothermic DSC peak at about 189 °C, which can be attributed to dehydration of four and a half water molecules from $CuFe_2(C_2O_4)_3{\cdot}4.5H_2O$ and the formation of $CuFe_2(C_2O_4)_3$. The observed mass loss in the TG curve is 15.72%, which is in good agreement with 15.58% theoretic mass loss of dehydration of four and a half water molecules from $CuFe_2(C_2O_4)_3{\cdot}4.5H_2O$. The second decomposition step begins at about 201 °C and ends at about 300 °C, which involves an exothermic process with a strong DSC peak at about 248 °C, attributed to the decomposition of $CuFe_2(C_2O_4)_3$ and the formation of $CuFe_2O_4$. The thermal decomposition of second step only requires about 22 °C from the beginning to finish, indicating that decomposition of $CuFe_2(C_2O_4)_3$ into $CuFe_2O_4$ in air is a fast step, which can be attributed that Fe^{2+} and Cu^{2+} ions with d^{6-9} outer electron configuration have strong polarization force. The corresponding observed mass loss in the TG curve is 36.56%, which is close to 38.45% theoretic mass loss of reaction of $CuFe_2(C_2O_4)_3$ with two O_2 molecules. The thermal process of third step is

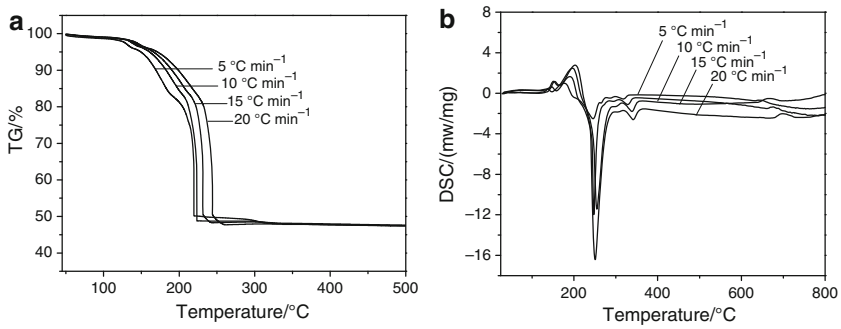

Fig. 1 TG/DSC curves of the $CuFe_2(C_2O_4)_3{\cdot}4.5H_2O$ at different heating rates in air

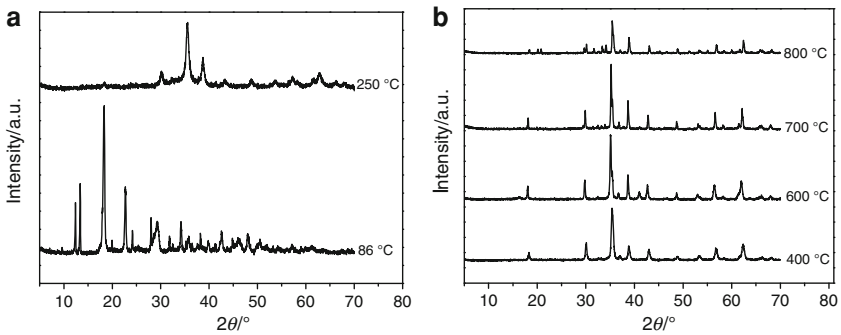

Fig. 2 XRD patterns of $CuFe_2(C_2O_4)_3{\cdot}4.5H_2O$ and its calcined samples at different temperatures in air for 1 h

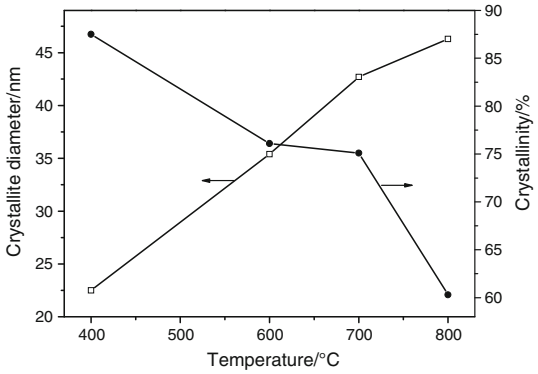

Fig. 3 Crystallite diameters and crystallinity of $CuFe_2O_4$

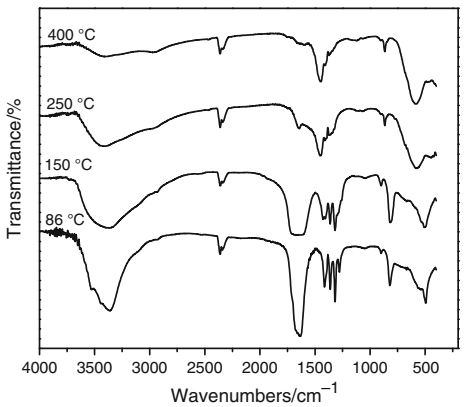

Fig. 4 FT-IR spectra of $CuFe_2(C_2O_4)_3{\cdot}4.5H_2O$ and its calcined samples

crystallization of cubic $CuFe_2O_4$ and characterized by a weak exothermic DSC peak at about 328 °C.

XRD analysis of $CuFe_2(C_2O_4)_3{\cdot}4.5H_2O$ and its calcined samples

Figure 2 shows the XRD patterns of $CuFe_2(C_2O_4)_3{\cdot}4.5H_2O$ dried at 86 °C and the calcined products at different temperatures in air for 1 h.

From Fig. 2a, the results show that strong intensity and smoothed baseline, a wide and low diffraction pattern of the precursor is observed, which indicates that the $CuFe_2(C_2O_4)_3{\cdot}6H_2O$ obtained at 86 °C is a crystalline with higher crystallinity. The diffraction peaks in the pattern can be indexed to be in agreement with the orthorhombic $FeC_2O_4{\cdot}2H_2O$ from PDF card 23-0293, with space group 12/a(15). No diffraction peaks of copper oxalate, such as CuC_2O_4 or $CuC_2O_4{\cdot}xH_2O$, are observed, which implies that Cu^{2+} ions enter lattice of $FeC_2O_4{\cdot}2H_2O$, and CuC_2O_4 or $CuC_2O_4{\cdot}xH_2O$ forms a solid solution with $FeC_2O_4{\cdot}2H_2O$. It is explained by the fact that Cu^{2+} ion (72 pm) and Fe^{2+} ion (75 pm) have same electric charge and similar ionic radius. When the precursor is calcined at 250 °C for 1 h, a part of characteristic diffraction peaks of cubic $CuFe_2O_4$ with weak intensity is observed. From Fig. 2b, when the sample was heated at 400 °C in air for 1 h, the diffraction peaks in the pattern are in agreement with those of cubic $CuFe_2O_4$, with space group F, lattice parameters: $a = b = c = 0.8349$ nm, $\alpha = \beta = \gamma = 90^{o}$, density $= 5.31$ g cm^{-3}, from PDF card 25-0283. Intensity of diffraction peaks of impurities, such as CuO and Fe_2O_3, increases with increasing calcination temperature.

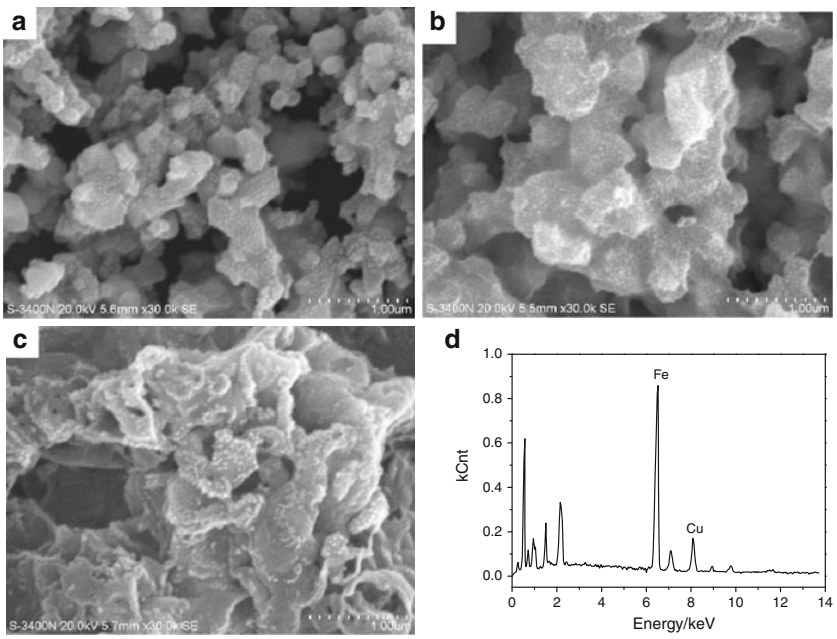

Fig. 5 SEM and EDS analyses of the calcined sample: **a** 600 °C, **b** 700 °C, **c** 800 °C

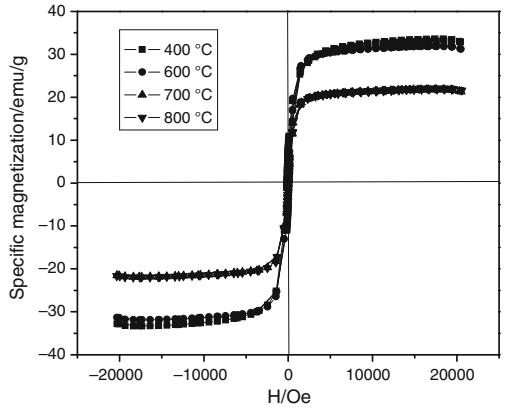

Fig. 6 Hysteresis loops for $CuFe_2O_4$ samples obtained at different temperatures in air for 1 h

According to the Scherrer formula [6]: $D = K\lambda/(\beta\cos\theta)$, where D is crystallite diameter, $K = 0.89$ (the Scherrer constant), $\lambda = 0.15406$ nm (wavelength of the X-ray used), β is the width of line at the half-maximum intensity, and θ is the corresponding angle. The resulting crystallite sizes of the products from calcining precursor can be obtained. Besides, the crystallinity of cubic $CuFe_2O_4$ can be calculated via MDI Jade 5.0 software [28]. The results are shown in Fig. 3. From Fig. 3, it can be seen that the crystallite sizes of the products increase with increasing calcination temperature. However, the crystallinity of cubic $CuFe_2O_4$ decreases with increasing calcination temperature, which is attributed that the cubic $CuFe_2O_4$ can decompose into CuO and Fe_2O_3 above 400 °C. In other words, cubic $CuFe_2O_4$ is thermodynamically more stable at 400 °C.

IR spectroscopic analysis of $CuFe_2(C_2O_4)_3{\cdot}4.5H_2O$ and its calcined samples

The FT-IR spectra of $CuFe_2(C_2O_4)_3{\cdot}4.5H_2O$ and its calcined sample are shown in Fig. 4. The $CuFe_2(C_2O_4)_3{\cdot}4.5H_2O$ exhibits a strong and broad band at about 3,400 cm^{-1} that can be assigned to the stretching OH vibration of the water molecule. The weak band at about 827 cm^{-1} is the water libration (hindered rotation). The strong band, which appears at 1,643 cm^{-1} in the spectrum of the precursor, can be ascribed to the bending mode of the HOH [6, 19, 28]. The bands at 1,338 cm^{-1} can be assigned to either the appearance of new M–OC_2O_3 (M = Cu, Fe) bonds and/or to the combinations of OH librations and lattice modes [6, 24]. When $CuFe_2(C_2O_4)_3{\cdot}4.5H_2O$ is calcined at 400 °C, the bands at 2,361 and 1,453 cm^{-1} are attributed to the absorption of CO_2 and absorption of water from air, respectively.

Table 1 Correlative data of thermal process of $CuFe_2(C_2O_4)_3{\cdot}4.5H_2O$ for step 1

α	β/K min^{-1}			
	5 (*T*/K)	10 (*T*/K)	15 (*T*/K)	20 (*T*/K)
0.2	405	415	419	422
0.3	420	432	437	442
0.4	429	441	447	453
0.5	436	448	455	462
0.6	441	454	461	469
0.7	445	459	467	476
0.8	449	464	473	482

Table 2 Correlative data of thermal process of $CuFe_2(C_2O_4)_3{\cdot}4.5H_2O$ for step 2

α	β/K min^{-1}			
	5 (*T*/K)	10 (*T*/K)	15 (*T*/K)	20 (*T*/K)
0.1	477	485	494	502
0.2	484	491	499	508
0.3	487	494	501	511
0.4	489	496	504	513
0.5	491	498	505	516
0.6	493	499	508	517

SEM and EDS analyses of the calcined samples

The morphologies and EDS spectrum of the calcined samples are shown in Fig. 5. From Fig. 5a, it can be seen that the calcined sample obtained at 600 °C is composed of irregular grains, there is a soft agglomeration phenomenon in the particles of sample, and the observed particles sizes are between 100 and 300 nm. With the increase in calcination temperature, the calcined sample is aggregated into larger grains further. Figure 5c shows the SEM micrographs of sample obtained at 800 °C. It can be seen that the calcined sample obtained at 800 °C becomes lamellar shape. The average crystallite sizes of the calcined samples determined by X-ray diffraction are significantly smaller than the values determined by SEM. This is attributed that values observed by SEM technique give the size of the secondary particles, and the X-ray line broadening analysis discloses only the size of primary particles. Figure 5d shows EDS spectrum of the calcined product obtained at 700 °C, and the result shows that mole ratio of Cu/Fe is equal to 0.95:2.15, which closes to that obtained by XRD analysis.

Magnetic properties of the calcined samples

Figure 6 shows the hysteresis loops of the $CuFe_2O_4$ particles obtained at different calcination temperatures. From

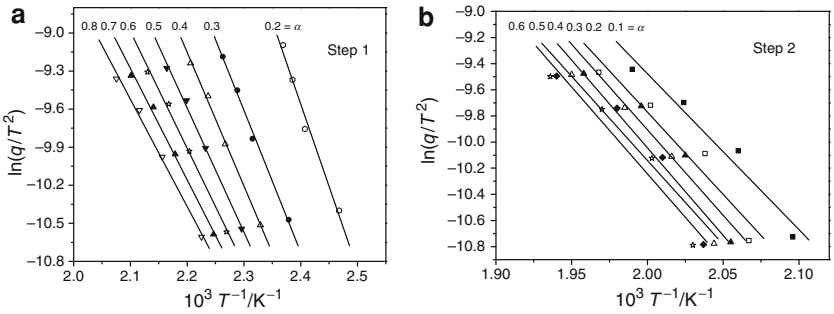

Fig. 7 Isoconversional plots at various conversion degrees for $CuFe_2(C_2O_4)_3{\cdot}4.5H_2O$ draw according KAS calculation procedure

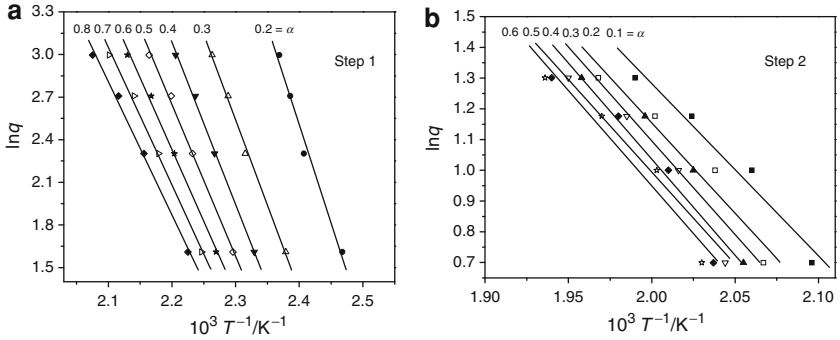

Fig. 8 Isoconversional plots at various conversion degrees for $CuFe_2(C_2O_4)_3{\cdot}4.5H_2O$ draw according OFW calculation procedure

Table 3 The activation energies (E_a) and intercept (B) for thermal decomposition of $CuFe_2(C_2O_4)_3{\cdot}4.5H_2O$ at different conversion degree and calculating procedure for step 1

Conversion degree/α	E_a/kJ mol^{-1}				B	
	KAS method	OFW method	$\ln[q/(h(x)T^2)] \sim 1/T$	$\ln[q/H(x)] \sim 1/T$	Eq. 3	Eq. 4
0.2	108	109	108	108	21.78798	35.39991
0.3	93	95	93	93	16.22387	29.53228
0.4	88	90	88	88	14.17575	27.36788
0.5	81	84	82	82	12.09366	25.13863
0.6	77	80	77	77	10.52195	23.44680
0.7	73	77	73	73	9.336010	22.16611
0.8	70	74	71	71	8.433090	21.19028
Average	84 ± 24	87 ± 22	85 ± 23	85 ± 23	13.22461	26.32027

$\ln[q/(h(x)T^2)] \sim 1/T$ and $\ln[q/H(x)] \sim 1/T$ are the iterative results of KAS method and OFW method, respectively. B is the intercept of the plots of Eqs. 3 and 4

Fig. 6, it can be observed that specific saturation magnetizations of powders calcined at 400, 600, 700, and 800 °C for 1 h are 33.5, 31.9, 21.8, and 22.0 emu g^{-1}, respectively. That is, specific saturation magnetization decreases with increasing calcination temperature. In other words, the smaller the crystallinity of the particles, the smaller is the specific saturation magnetizations. The smaller Ms values associated with smaller crystallinity can be explained as follows: First, $CuFe_2O_4$ can decompose into CuO and Fe_2O_3 particles with weak magnetic intensity above 400 °C, and weak magnetic CuO and Fe_2O_3 particles can reduce the net magnetic moment in the samples. Second, the magnetocrystalline anisotropy of the particles is dependent on the crystallinity of $CuFe_2O_4$. When the calcination temperature increases, the crystallinity of particles decreases, which increases magnetocrystalline anisotropy distortion and decreases magnetic moment within the particles of $CuFe_2O_4$ [10].

Kinetics of thermal decomposition of $CuFe_2(C_2O_4)_3{\cdot}4.5H_2O$

In accordance with TG/DSC and XRD analyses of $CuFe_2(C_2O_4)_3{\cdot}4.5H_2O$ and its calcined products mentioned

Table 4 The activation energies (E_a) and intercept (B) for thermal decomposition of $CuFe_2(C_2O_4)_3{\cdot}4.5H_2O$ at different conversion degree and calculating procedure for step 2

Conversion degree/α	E_a/kJ mol^{-1}				B	
	KAS method	OFW method	$\ln[q/(h(x)T^2)] \sim 1/T$	$\ln[q/H(x)] \sim 1/T$	Eq. 3	Eq. 4
0.1	99	102	100	100	14.57970	28.02413
0.2	104	107	105	105	15.44839	28.98788
0.3	109	112	109	109	16.49216	30.12324
0.4	112	114	112	112	16.91024	30.58370
0.5	107	110	107	107	15.76294	29.35658
0.6	110	113	111	111	16.41293	30.06367
Average	107 ± 8	110 ± 8	107 ± 7	107 ± 7	15.93439	29.52320

above, thermal process of $CuFe_2(C_2O_4)_3{\cdot}4.5H_2O$ below 400 °C consists of three steps, which can be expressed as follows, respectively.

$$CuFe_2(C_2O_4)_3 \cdot 4.5H_2O(cr) \rightarrow CuFe_2(C_2O_4)_3(cr) + 4.5H_2O(g) \quad (8)$$

$$CuFe_2(C_2O_4)_3(cr) + 2O_2(g) \rightarrow CuFe_2O_4(am) + 6CO_2(g) \quad (9)$$

$$CuFe_2O_4(am) \rightarrow CuFe_2O_4(c) \quad (10)$$

According to non-isothermal method, the basic data of α and T collected from the TG curves of the thermal decomposition of $CuFe_2(C_2O_4)_3{\cdot}4.5H_2O$ at various heating rates (5, 10, 15, and 20 K min^{-1}) are illustrated in Tables 1 and 2.

According to Eqs. 1 and 2, the isoconversional calculation procedures of KAS and OFW are used. The corresponding KAS and OFW lines obtained at different conversion degrees α and different heating rates q are shown in Figs. 7 and 8, respectively.

The values of the activation energies associated with the thermal process of $CuFe_2(C_2O_4)_3{\cdot}4.5H_2O$ for the first thermal process step corresponding to different conversions α are obtained by the KAS and OFW calculation procedure and the iterative method mentioned above. The results are shown in Tables 3 and 4, respectively.

From Tables 3 and 4, E_a values for thermal decomposition of step 1 obtained by iterative method are very close to those obtained by KAS method (differing about 1 kJ mol^{-1}), and those by OFW method is higher than those obtained by iterative method (differing about 2 kJ mol^{-1}). E_a values for thermal decomposition of step 2 obtained by iterative method are very close to those obtained by KAS method (differing about 0 kJ mol^{-1}), and those by OFW method is higher than those obtained by iterative method (differing about 3 kJ mol^{-1}). However, it can be discovered that the E_a values obtained from the plot of $\ln[q/H(x)]$ versus $1/T$ or $\ln[q/(h(x)T^2)]$ versus $1/T$ by iterative procedure are very close to each other. From Tables 3 and 4, the activation energies change in the step 1 with α is higher than 10%, and that in the step 2 with α is lower than 10%, so that we draw a conclusion that the dehydration of the crystal water of $CuFe_2(C_2O_4)_3{\cdot}4.5H_2O$ could be multistep reaction mechanism, and decomposition of $CuFe_2(C_2O_4)_3$ into $CuFe_2O_4$ could be simple reaction mechanism [19, 27, 29, 30].

According to Eq. 2 and Table 2, conversion degree and temperature corresponding to heating rate are put into twenty-six types of mechanism functions, respectively. The slope k, correlation coefficient r, and intercept B of linear regression of ln [$g(\alpha)$] versus ln q are obtained. Mechanism function, in which the value of k is closest to −1.00000 and the correlation coefficient r^2 is higher, is chosen as mechanism function of thermal decomposition of $CuFe_2(C_2O_4)_3$. The results show that probable mechanism function integral form of thermal decomposition of $CuFe_2(C_2O_4)_3$ is determined to be $g(\alpha) = 1 - (1 - \alpha)^{1/4}$.

The pre-exponential factor A is estimated from the intercept of the plots of Eq. 2 by inserting the most probable $g(\alpha)$ function determined. The results show that the range of pre-exponential factor A is 1.86×10^{10} min^{-1}.

Conclusions

We have successfully synthesized nanocrystalline $CuFe_2O_4$ via a novel and simple method. XRD analysis shows that precursor is a solid solution containing $CuFe_2(C_2O_4)_3{\cdot}4.5H_2O$. Crystalline $CuFe_2O_4$ with cubic structure is obtained when the precursor is calcined above 400 °C in air for 1 h. Magnetic characterization indicates that the specific saturation magnetization of $CuFe_2O_4$ obtained at 400 °C is 33.5 emu g^{-1}. The thermal process of the precursor in the range of ambient temperature to 400 °C experiences three steps, which involves the dehydration of the waters of crystallization at first; then the decomposition of $CuFe_2(C_2O_4)_3$ and formation of amorphous $CuFe_2O_4$; and at last crystallization of cubic $CuFe_2O_4$. The kinetics of

the thermal process of the precursor is studied using TG/DSC technique. The values of the activation energy for the thermal process of $CuFe_2(C_2O_4)_3{\cdot}4.5H_2O$ are determined to be 85 ± 23 and 107 ± 7 kJ mol^{-1} for the first and second thermal process steps, respectively. Dehydration of $CuFe_2(C_2O_4)_3{\cdot}4.5H_2O$ is multistep reaction mechanisms, and decomposition of $CuFe_2(C_2O_4)_3$ into $CuFe_2O_4$ could be simple reaction mechanism.

Acknowledgements This study was financially supported by the National Nature Science Foundation of China (Grant no. 21161002) and the Guangxi Nature Science Foundation of China (Grant no. 2011GXNSFA018036).

References

1. Sugimoto M. The past, present, and future of ferrites. J Am Ceram Soc. 1999;82:269–80.
2. Raj K, Moskowitz B, Casciari R. Advances in ferrofluid technology. J Magn Magn Mater. 1995;149:174–80.
3. McMichael RD, Shull RD, Swartzendruber LJ, Bennett LH, Watson RE. Magnetocaloric effect in superparamagnets. J Magn Magn Mater. 1992;111:29–33.
4. Sun ZP, Liu L, Jia DZ, Pan WY. Simple synthesis of $CuFe_2O_4$ nanoparticles as gas-sensing materials. Sens Actuators B. 2007;125:144–8.
5. Li JJ, Yuan HM, Li GD, Liu YJ, Leng JS. Cation distribution dependence of magnetic properties of sol–gel prepared $MnFe_2O_4$ spinel ferrite nanoparticles. J Magn Magn Mater. 2010;322:3396–400.
6. Wu XH, Wu WW, Zhou KW, Cui XM, Liao S. Products and non-isothermal kinetics of thermal decomposition of $MgFe_2(C_2O_4)_3{\cdot}6H_2O$. J Therm Anal Calorim. 2011. doi:10.1007/s10973-011-1968-9.
7. Li FS, Wang HB, Wang L, Wang JB. Magnetic properties of $ZnFe_2O_4$ nanoparticles produced by a low-temperature solid-state reaction method. J Magn Magn Mater. 2007;309:295–9.
8. Wu WW, Cai JC, Wu XH, Li YN, Liao S. Magnetic properties and crystallization kinetics of $Zn_{0.5}Ni_{0.5}Fe_2O_4$. Rare Met. 2011. doi:10.1007/s12598-011-0439-6.
9. Satyanarayana L, Madhusudan Reddy K, Manorama SV. Nanosized spinel $NiFe_2O_4$: a novel material for the detection of liquefied petroleum gas in air. Mater Chem Phys. 2003;82:21–6.
10. Zhang K, Holloway T, Pradhan AK. Magnetic behavior of nanocrystalline $CoFe_2O_4$. J Magn Magn Mater. 2011;323:1616–22.
11. Wu WW, Cai JC, Wu XH, Liao S, Huang AG. $Co_{0.35}Mn_{0.65}Fe_2O_4$ magnetic particles: preparation and kinetics research of thermal process of the precursor. Powder Technol. 2011. doi:10.1016/j.powtec.2011.09.048.
12. Goya GF, Rechenberg HR. Superparamagnetic transition and local disorder in $CuFe_2O_4$ nanoparticles. Nanostruct Mater. 1998;10:1001–11.
13. Jiang JZ, Goya GF, Rechenberg HR. Magnetic properties of nanostructured $CuFe_2O_4$. J Phys Condens Mater. 1999;11:4063–78.
14. Bomio M, Lavela P, Tirado JL. Electrochemical evaluation of $CuFe_2O_4$ samples obtained by sol–gel methods used as anodes in lithium batteries. J Solid State Electrochem. 2008;12:729–37.
15. Pandya PB, Joshi HH, Kulkarni RG. Magnetic and structural properties of $CuFe_2O_4$ prepared by the co-precipitation method. J Mater Sci Lett. 1991;10:474–6.
16. Tao SW, Gao F, Liu XQ, Sørensen OT. Preparation and gas-sensing properties of $CuFe_2O_4$ at reduced temperature. Mater Sci Eng B. 2000;77:172–6.
17. Zhang YS, Stangle GC. Preparation of fine multicomponent oxide ceramic powder by a combustion synthesis process. J Mater Res. 2004;9:1997–2004.
18. Vanetsev AS, Ivanov VK, Tret'yakov Yu D. Microwave synthesis of lithium, copper, cobalt, and nickel ferrites. Dokl Chem. 2002;387:332–4.
19. Wu XH, Wu WW, Li SS, Cui XM, Liao S. Kinetics and thermodynamics of thermal decomposition of $NH_4NiPO_4{\cdot}6H_2O$. J Therm Anal Calorim. 2011;103:805–12.
20. Chrissafis K. Kinetics of thermal degradation of polymers. Complementary use of isoconversional and model-fitting methods. J Therm Anal Calorim. 2009;95:273–83.
21. Chen ZP, Chai Q, Liao S, He Y, Wu WW, Li B. Preparation of $LiZnPO_4{\cdot}H_2O$ via a novel modified method and its non-isothermal kinetics and thermodynamics of thermal decomposition. J Therm Anal Calorim. 2011. doi:10.1007/s10973-011-1799-8
22. Ozawa T. A new method of analyzing thermogravimetric data. Bull Chem Soc Jpn. 1965;38:1881–6.
23. Flynn JH. The 'temperature integral'—its use and abuse. Thermochim Acta. 1997;300:83–92.
24. Vlaev L, Nedelchev N, Gyurova K, Zagorcheva M. A comparative study of non-isothermal kinetics of decomposition of calcium oxalate monohydrate. J Anal Appl Pyrolysis. 2008;81:253–62.
25. Senum GI, Yang RT. Rational approximations of the integral of the Arrhenius function. J Therm Anal. 1977;11:445–7.
26. Liqing L, Donghua C. Application of iso-temperature method of multiple rate to kinetic analysis. Dehydration for calcium oxalate monohydrate. J Therm Anal Calorim. 2004;78:283–93.
27. Genieva SD, Vlaev LT, Atanassov AN. Study of the thermo-oxidative degradation kinetics of poly(tetrafluoroethene) using iso-conversional calculation procedure. J Therm Anal Calorim. 2010;99:551–61.
28. Liu C, Wu XH, Wu WW, Cai JC, Liao S. Preparation of nanocrystalline $LiMnPO_4$ via a simple and novel method and its isothermal kinetics of crystallization. J Mater Sci. 2011;46:2474–8.
29. Boonchom B, Danvirutai C. Kinetics and thermodynamics of thermal decomposition of synthetic $AlPO_4{\cdot}2H_2O$. J Therm Anal Calorim. 2009;98:771–7.
30. Wu WW, Li YN, Zhou KW, Wu XH, Liao S, Wang Q. Nanocrystalline $Zn_{0.5}Ni_{0.5}Fe_2O_4$: preparation and kinetics of thermal process of precursor. J Therm Anal Calorim. 2011. doi:10.1007/s10973-011-2027-2.